



**Disruption of Vertical Motility by Shear Triggers
Formation of Thin Phytoplankton Layers**

William M. Durham, *et al.*
Science **323**, 1067 (2009);
DOI: 10.1126/science.1167334

**The following resources related to this article are available online at
www.sciencemag.org (this information is current as of February 19, 2009):**

Updated information and services, including high-resolution figures, can be found in the online version of this article at:

<http://www.sciencemag.org/cgi/content/full/323/5917/1067>

Supporting Online Material can be found at:

<http://www.sciencemag.org/cgi/content/full/323/5917/1067/DC1>

This article **cites 29 articles**, 3 of which can be accessed for free:

<http://www.sciencemag.org/cgi/content/full/323/5917/1067#otherarticles>

This article appears in the following **subject collections**:

Ecology

<http://www.sciencemag.org/cgi/collection/ecology>

Information about obtaining **reprints** of this article or about obtaining **permission to reproduce this article** in whole or in part can be found at:

<http://www.sciencemag.org/about/permissions.dtl>

Disruption of Vertical Motility by Shear Triggers Formation of Thin Phytoplankton Layers

William M. Durham,¹ John O. Kessler,² Roman Stocker^{1*}

Thin layers of phytoplankton are important hotspots of ecological activity that are found in the coastal ocean, meters beneath the surface, and contain cell concentrations up to two orders of magnitude above ambient concentrations. Current interpretations of their formation favor abiotic processes, yet many phytoplankton species found in these layers are motile. We demonstrated that layers formed when the vertical migration of phytoplankton was disrupted by hydrodynamic shear. This mechanism, which we call gyrotactic trapping, can be responsible for the thin layers of phytoplankton commonly observed in the ocean. These results reveal that the coupling between active microorganism motility and ambient fluid motion can shape the macroscopic features of the marine ecological landscape.

Advances in underwater sensing technology over the past three decades have revealed the occurrence throughout the oceans of intense assemblages of unicellular photosynthetic organisms known as thin layers. Thin layers are centimeters to meters thick (1) and extend horizontally for kilometers (2). They often occur in coastal waters (1–4), in regions of vertical gradients in density where they are partially sheltered from turbulent mixing (1), and can persist for hours to days (2, 5–7). Thin phytoplankton layers contain elevated amounts of

marine snow and bacteria (6, 8), enhance zooplankton growth rates (7), and provide the prey concentrations essential for the survival of some fish larvae (9). On the other hand, because many phytoplankton species found in these layers are toxic (2, 3, 5, 10, 11), thin layers can disrupt grazing, enhance zooplankton and fish mortality, and seed harmful algal blooms at the ocean surface (2, 5, 10). The large biomass found in thin layers can influence optical and acoustic signatures in the ocean (1, 6, 8). Understanding the mechanisms driving thin layer formation is

critical for predicting their occurrence and ecological ramifications.

Phytoplankton species found in thin layers are often motile (2, 3, 5, 9, 11). The interplay between motility and fluid flow can result in complex and ecologically important phenomena, including localized cell accumulations (12, 13) and directed swimming against the flow in zooplankton (13), bacteria (14), and sperm (15). Phytoplankton motility, coupled with shear, can lead to a striking focusing effect known as gyrotaxis (12). Shear, in the form of vertical gradients in horizontal fluid velocity, can be generated by tidal currents (1), wind stress (1), and internal waves (16) and is often enhanced within thin layers (4, 17). Here, we propose a mechanism for thin layer formation in which a population of motile phytoplankton accumulates where shear exceeds a critical threshold: We have called this phenomenon gyrotactic trapping.

Many phytoplankton species exhibit gravitaxis, a tendency to swim upward against gravity. Gravitaxis can result from a torque caused by asymmetry in shape (18) or in distribution of body density (12) or through active sensing (19). Hydrodynamic shear imposes a viscous torque

¹Department of Civil and Environmental Engineering, Massachusetts Institute of Technology (MIT), Cambridge, MA 02139, USA. ²Department of Physics, University of Arizona, Tucson, AZ 85721, USA.

*To whom correspondence should be addressed. E-mail: romans@mit.edu

Fig. 1. Gyrotactic trapping. (A) A gyrotactic phytoplankton's center of mass (red) is displaced from its center of buoyancy ($x = z = 0$). As a result, the swimming direction θ in a shear flow, $u(z)$, is set by the balance of gravitational (T_g) and viscous (T_v) torques. V is swimming speed and m is mass. (B) Schematic of gyrotactic trapping. Cells can migrate vertically at low shear but tumble and become trapped where $|S| > S_{CR}$, accumulating in a thin layer. (C) Experimental apparatus to test gyrotactic trapping. The rotating belt generated a depth-varying shear $S(z)$ in the underlying flow chamber.

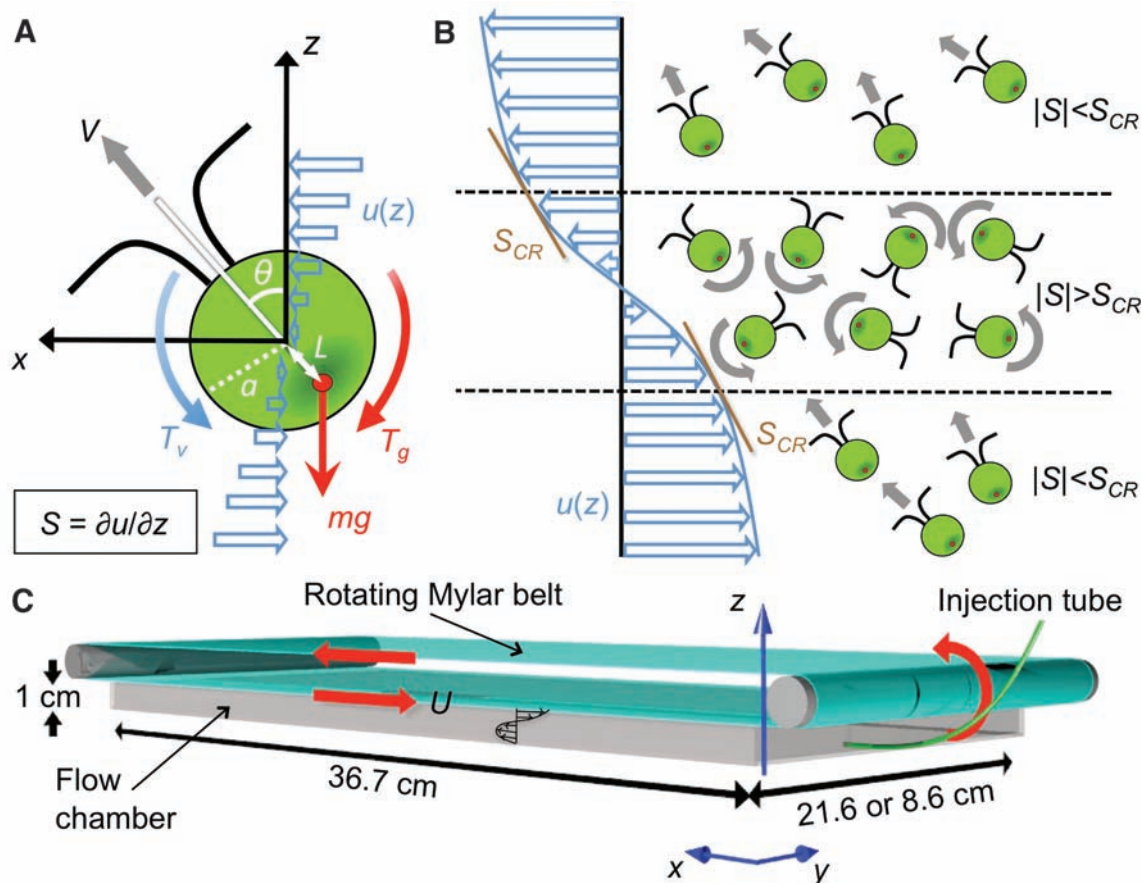
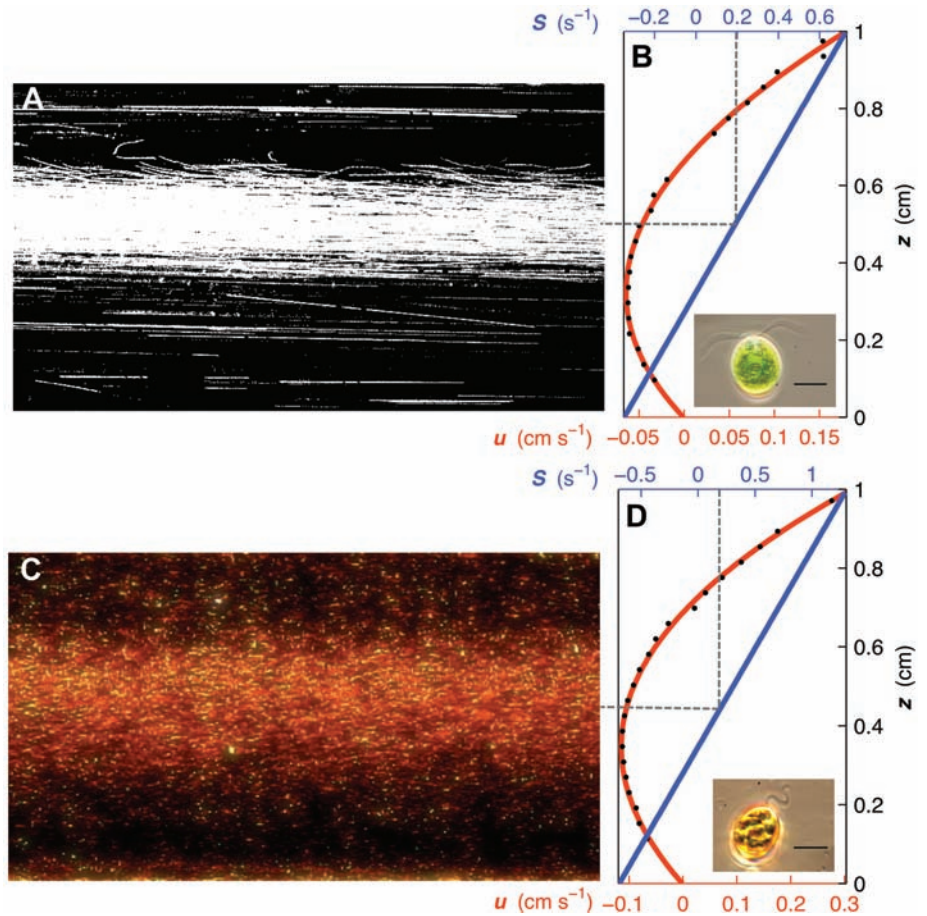


Fig. 2. Thin phytoplankton layers. **(A)** Multiple-exposure image showing a thin layer of *C. nivalis* ($t = 12$ min, $x = 21.5$ cm). Cells in high shear ($z > 0.5$ cm) were trapped, whereas those beneath ($|S| < S_{CR}$) swam upward, forming a thin layer. **(B)** Corresponding profile of measured flow velocities u (black dots), along with a quadratic fit (red) and the associated shear $S = \partial u / \partial z$ (blue). Because $u(z)$ was parabolic, S increased linearly with z . (Inset) *C. nivalis*, showing the two flagella used for swimming. Scale bar indicates $10 \mu\text{m}$. **(C)** Thin layer of *H. akashiwo*. **(D)** Same as (B), for experiments in Fig. 2C. (Inset) *H. akashiwo*, showing one flagellum (a second resides in a ventral groove). Scale bar, $10 \mu\text{m}$.



on cells. The swimming direction, θ , is then set by the balance of viscous and gravitactic torques (Fig. 1A), and cells are said to be gyrotactic (12). Consider a spherical cell of radius a and mean density ρ (Fig. 1A), with an asymmetric density distribution creating an offset, L , between its center of mass and its center of buoyancy (an equivalent L can be used to characterize gravitaxis resulting from shape or sensing). When exposed to shear S , the cell swims upward in the direction $\sin\theta = BS(12)$, where $B = 3\mu/\rho Lg$ is the gyrotactic reorientation time scale, μ the dynamic fluid viscosity, and g the acceleration of gravity. This results from the vorticity component of shear, whereas elongated cells would further be affected by the rate of strain component.

We show that vertical gradients ($S = \partial u / \partial z$) in horizontal velocity u can disrupt vertical migration of gyrotactic phytoplankton, causing them to accumulate in layers. When $|S| > S_{CR} = B^{-1}$, the stabilizing gravitational torque that acts to orient cells upward is overwhelmed by the hydrodynamic torque that induces them to spin: Upward migration is disrupted, because no equilibrium orientation exists ($|\sin\theta|$ must be ≤ 1), and cells tumble end over end, accumulating where they tumble (Fig. 1B). We demonstrated that gyrotactic trapping triggers layer formation by exposing the green alga *Chlamydomonas nivalis* and the toxic raphidophyte *Heterosigma akashiwo* (Fig.

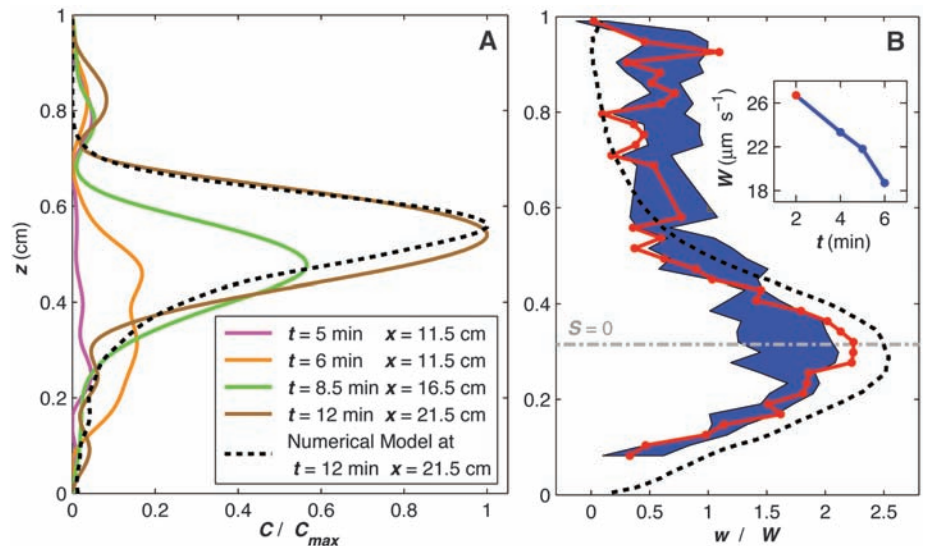


Fig. 3. Formation of a thin layer. **(A)** Cell concentration profiles $C(z)$ observed experimentally (solid lines) and numerically (dashed line), normalized by C_{max} observed at $t = 12$ min, $x = 21.5$ cm. **(B)** Upward swimming speed, w , at $t = 2$ min (red line) and standard deviation across four observations (blue strip and inset). W is the depth-averaged value of w . The dashed line shows the numerical simulation. The peak in $w(z)$ at $S \approx 0$ (gray line) and the deterioration in $w(z)$ for $|S| > 0$ are consistent with gyrotaxis and were responsible for layer formation. (Inset) W decreased with time, as the proportion of cells reaching their critical shear rate increased.

2, B and D, insets) to a linearly varying shear, $S(z)$ (Fig. 2, B and D), in a 1-cm-deep chamber (Fig. 1C). *C. nivalis* is a classic model for gyrotaxis (12), whereas *H. akashiwo* has been the

culprit of numerous large-scale fish kills and is known to form thin layers (11).

In our experiments, *C. nivalis* consistently formed intense thin layers (Fig. 2A). The dynamics

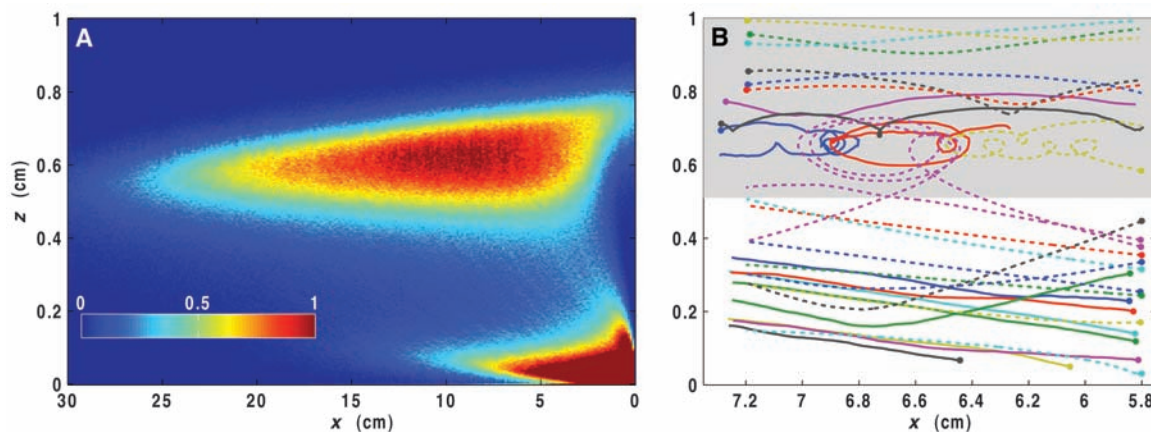


Fig. 4. Cell accumulation and trajectories. **(A)** Thin layer obtained from the numerical model at $t = 12$ min for conditions that simulated experiments with *C. nivalis* (Fig. 3A). Color denotes normalized cell concentration (the high concentrations at the lower right represent the region of injection). **(B)** Transition between two swimming regimes,

demonstrated by experimental (solid) and numerical (dashed) trajectories. Where $|S| < S_{CR}$ (white background), cells migrated upward, whereas $|S| > S_{CR}$ (gray background) triggered tumbling and trapping. Shading represents the mean critical shear rate $S_{CR} = 0.2 \text{ s}^{-1}$, although a statistical variability existed among cells. Dots mark beginning of trajectories.

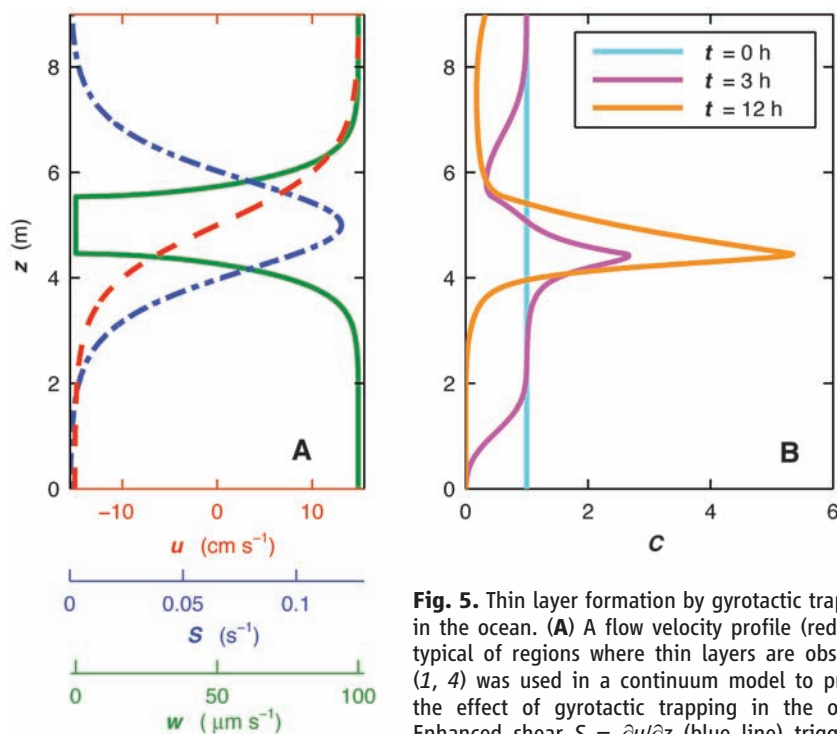


Fig. 5. Thin layer formation by gyrotactic trapping in the ocean. **(A)** A flow velocity profile (red line) typical of regions where thin layers are observed (1, 4) was used in a continuum model to predict the effect of gyrotactic trapping in the ocean. Enhanced shear $S = \partial u / \partial z$ (blue line) triggers a reduction in upward swimming speed w (green

line). **(B)** The model shows that an initially uniform population (cyan line) develops a localized accumulation within 3 hours (pink line) and forms an intense thin layer within 12 hours (orange line). Turbulence was parameterized by a vertical eddy diffusivity $D = 10^{-5} \text{ m}^2 \text{ s}^{-1}$.

of thin layer formation were captured by using video microscopy (Fig. 3A). Initially (time $t = 6$ min, horizontal position $x = 11.5$ cm), cells entered the field of view with a broad distribution. Subsequently ($t = 8.5$ min, $x = 16.5$ cm), a 4-mm-wide thin layer formed as a result of the uppermost cells becoming trapped where $S_{CR} \approx 0.2 \text{ s}^{-1}$ and the cells beneath them still swimming upward. The location of cell accumulation corresponded to a gyrotactic reorientation time $B = 1/S_{CR} \approx 5$ s, in good agreement with previous

literature values [$B \approx 1$ to 6 s (20, 21, 22)]. The thin layer grew more intense over time, peaking at $t = 12$ min. Importantly, motility was critical for layer formation: No layers were observed to form when we used dead cells. *H. akashiwo* also produced thin layers, which were so intense that they were visible to the naked eye (Fig. 2C), at a depth corresponding to $S_{CR} \approx 0.5 \text{ s}^{-1}$.

Was gyrotaxis the mechanism underlying layer formation? According to theory, the mean upward speed, w , of a population of gyrotactic

cells decreases with increasing shear. Measured vertical profiles of $w(z)$ from 70,000 *C. nivalis* trajectories (Fig. 3B) strongly support the occurrence of gyrotactic trapping: $w(z)$ peaked at $S = 0$ and decreased above and below. These observations were corroborated by numerical simulations of 50,000 cell trajectories under conditions mimicking the experiments (23) (movie S1). The simulations resulted in the formation of an intense thin layer (Fig. 4A), with cell concentration $C(z)$ closely matching observations (Fig. 3A). Furthermore, $w(z)$ decayed with increasing S , as in experiments (Fig. 3B).

Gyrotactic trapping requires a transition in swimming kinematics when $|S| = S_{CR}$ for a thin layer to form. To verify the existence of this transition, we tracked individual *C. nivalis* cells. Trajectories clearly revealed two distinct regimes (Fig. 4B and movie S2): for $|S| < S_{CR}$, cells swam upward, whereas for $|S| > S_{CR}$ they tumbled. Numerical and experimental trajectories exhibited clear similarities in the amplitude and frequency of tumbles, the rate of upward swimming for $|S| < S_{CR}$, and the presence of cells temporarily expelled from the lower side of the layer only to swim back upward moments later.

Can gyrotactic trapping contribute to layer formation in the ocean, where vertical distances are of the order of meters and turbulence may destroy vertical heterogeneity? To find out, we developed a continuum model of cell concentration, C , in the upper 10 m of the ocean, starting with a uniform distribution and accounting for turbulence intensities typical of thin layers (24) via a uniform eddy diffusivity, $D = 10^{-5} \text{ m}^2 \text{ s}^{-1}$. Even for a conservatively low maximum upward swimming speed $w_{\max} = 100 \mu\text{m s}^{-1}$ (11, 25), phytoplankton began to accumulate just beneath the depth of maximum shear within three hours, and the intensity of the layer strengthened over 12 hours (Fig. 5B). These time scales are consistent with field observations (7). Turbulence

subsequently eroded the layer, reducing peak concentration by 50% after 30 hours. Consideration of a local reduction in eddy diffusivity, typically encountered at the pycnocline, further increases layer intensity and duration. Importantly, we predict layer formation for shear rates ($S = 0.12 \text{ s}^{-1}$) comparable to those observed in thin layers (up to $S = 0.088 \text{ s}^{-1}$) (1, 4), particularly considering that the latter likely underestimate peaks in shear because of coarse (meter-scale) sampling (1, 4). Furthermore, recent high-resolution measurements find S in excess of 0.5 s^{-1} in coastal waters (26), although the temporal coherence of these events remains to be determined.

Given the wide range of environmental conditions and species associated with thin layers, it is unlikely that a single mechanism is responsible for all layers (27). Although several mechanisms have been hypothesized, including in situ growth (24), buoyancy (27), and motility toward optimal resource levels (5), straining of a phytoplankton patch by shear is currently the most invoked (4, 16, 24, 27). Our findings offer an alternative explanation of the role of shear: Regions of enhanced shear disrupt vertical motility and trigger sharp-peaked cell accumulations *ex novo* (Fig. 5B). This could occur routinely in natural water bodies because many species of phytoplankton are gyrotactic (28). Contrary to straining, gyrotactic trapping predicts that a mixture of phytoplankton species with differing gyrotactic behavior (e.g., B) will be sorted into multiple monospecific layers at different depths: Such vertical species separation is often observed in the ocean (29) and can affect zooplankton foraging and the spread of viral epidemics.

Gyrotactic trapping suggests that stabilization against tumbling might represent an evolutionarily selected trait for vertically migrating phytoplankton species. The parameter B^{-1} measures a cell's stability against overturning by shear. Whereas no stabilization ($B^{-1} = 0$) leaves the cell at the mercy of flow even at very small shear rates, stabilization is limited by biomechanical constraints (e.g., how bottom-heavy a cell can be) and excessive stabilization hinders maneuverability in exploiting nutrient patches and escaping predators. Although a simple model suggests that biomechanical constraints are not the only determinants of cell stability (23), further investigation is needed to establish the importance of stabilization in determining cell morphology.

The importance of motility in governing the spatial distribution of microorganisms in the ocean has been emphasized in recent years, chiefly for bacteria navigating patchy distributions of organic matter (30, 31). Here we have demonstrated that motility and shear can generate intense thin layer accumulations of phytoplankton by gyrotactic trapping. By focusing resources, thin layers shape ecological interactions and can significantly affect trophic transfer and biogeochemical fluxes (7). Our results reveal how prominent macroscopic

features of the marine landscape can originate from the microscopic coupling between flow and the motility of some of its smallest inhabitants.

References and Notes

- M. M. Dekshenieks *et al.*, *Mar. Ecol. Prog. Ser.* **223**, 61 (2001).
- T. G. Nielsen, T. Kjørboe, P. K. Bjørnsen, *Mar. Ecol. Prog. Ser.* **62**, 21 (1990).
- D. W. Townsend, N. R. Pettigrew, A. C. Thomas, *Deep-Sea Res. Part II Top. Stud. Oceanogr.* **52**, 2603 (2005).
- J. P. Ryan, M. A. McManus, J. D. Paduan, F. P. Chavez, *Mar. Ecol. Prog. Ser.* **354**, 21 (2008).
- P. K. Bjørnsen, T. G. Nielsen, *Mar. Ecol. Prog. Ser.* **73**, 263 (1991).
- M. A. McManus *et al.*, *Mar. Ecol. Prog. Ser.* **261**, 1 (2003).
- T. J. Cowles, R. A. Desiderio, M. Carr, *Oceanography* **11**, 4 (1998).
- A. L. Allredge *et al.*, *Mar. Ecol. Prog. Ser.* **233**, 1 (2002).
- R. Lasker, *Fish. Bull. (Washington)* **73**, 453 (1975).
- P. L. Donaghay, T. R. Osborn, *Limnol. Oceanogr.* **42**, 1283 (1997).
- S. Yamochi, T. Abe, *Mar. Biol. (Berl.)* **83**, 255 (1984).
- J. O. Kessler, *Nature* **313**, 218 (1985).
- A. Genin, J. S. Jaffe, R. Reef, C. Richter, P. J. S. Franks, *Science* **308**, 860 (2005).
- J. Hill, O. Kalkanci, J. L. McMurray, H. Koser, *Phys. Rev. Lett.* **98**, 068101 (2007).
- F. P. Bretherton, L. Rothchild, *Proc. R. Soc. London Ser. B* **153**, 490 (1961).
- P. J. S. Franks, *Deep-Sea Res. Part I Oceanogr. Res. Pap.* **42**, 75 (1995).
- T. J. Cowles, in *Handbook of Scaling Methods in Aquatic Ecology: Measurements, Analysis, Simulation*, L. Seuront, P. G. Strutton, Eds. (CRC, Boca Raton, FL, 2003), pp. 31–49.
- A. M. Roberts, F. M. Deacon, *J. Fluid Mech.* **452**, 405 (2002).
- M. Lebert, D. P. Häder, *Nature* **379**, 590 (1996).
- M. S. Jones, L. Le Baron, T. J. Pedley, *J. Fluid Mech.* **281**, 137 (1994).
- N. A. Hill, D. P. Häder, *J. Theor. Biol.* **186**, 503 (1997).
- T. J. Pedley, N. A. Hill, J. O. Kessler, *J. Fluid Mech.* **195**, 223 (1988).
- Materials and methods are available as supporting material on Science Online.
- D. A. Birch, W. R. Young, P. J. S. Franks, *Deep-Sea Res. Part I Oceanogr. Res. Pap.* **55**, 277 (2008).
- D. Kamykowski, R. E. Reed, G. J. Kirkpatrick, *Mar. Biol. (Berlin)* **113**, 319 (1992).
- J. G. Mitchell, H. Yamazaki, L. Seuront, F. Wolk, H. Li, *J. Mar. Syst.* **69**, 247 (2008).
- M. T. Stacey, M. A. McManus, J. V. Steinbeck, *Limnol. Oceanogr.* **52**, 1523 (2007).
- J. O. Kessler, *Prog. Phycol. Res.* **4**, 257 (1986).
- L. T. Mouritsen, K. Richardson, *J. Plankton Res.* **25**, 783 (2003).
- R. Stocker, J. R. Seymour, A. Samadani, D. E. Hunt, M. F. Polz, *Proc. Natl. Acad. Sci. U.S.A.* **105**, 4209 (2008).
- F. Azam, F. Malfatti, *Nat. Rev. Microbiol.* **5**, 782 (2007).
- We thank P. Franks, W. Young, D. Grünbaum, T. Cowles, R. Bearon, M. Bees, D. Häder, D. Anderson, M. McManus, and L. Karp-Boss for helpful discussions; T. Peacock for the loan of experimental equipment; T. Clay and S. Stransky for developing BacTrack; R. A. Cattolico for providing *H. akashiwo*; and J. Mitchell, E. DeLong, S. Chisholm, M. Polz, H. Neph, J. Seymour, J. Bragg, B. Kirkup, P. Reis, D. Birch, and S. Sunghwan for comments on the manuscript. W.M.D. acknowledges a National Defense Science and Engineering Graduate Fellowship. J.O.K. acknowledges support from Department of Energy grant W31-109-ENG38. R.S. acknowledges support from NSF (OCE 0526241 and OCE CAREER 0744641), MIT's Earth Systems Initiative, and a Doherty Professorship.

Supporting Online Material

www.sciencemag.org/cgi/content/full/323/5917/1067/DC1
Materials and Methods

References
Movies S1 and S2

17 October 2008; accepted 7 January 2009
10.1126/science.1167334

Cytosolic Viral Sensor RIG-I Is a 5'-Triphosphate-Dependent Translocase on Double-Stranded RNA

Sua Myong,^{1,†} Sheng Cui,^{2,*} Peter V. Cornish,^{3,4} Axel Kirchhofer,² Michaela U. Gack,^{5,6,7} Jae U. Jung,^{5,6} Karl-Peter Hopfner,^{2,†} Taekjip Ha^{1,3,4,†}

Retinoic acid inducible–gene I (RIG-I) is a cytosolic multidomain protein that detects viral RNA and elicits an antiviral immune response. Two N-terminal caspase activation and recruitment domains (CARDs) transmit the signal, and the regulatory domain prevents signaling in the absence of viral RNA. 5'-triphosphate and double-stranded RNA (dsRNA) are two molecular patterns that enable RIG-I to discriminate pathogenic from self-RNA. However, the function of the DEXH box helicase domain that is also required for activity is less clear. Using single-molecule protein-induced fluorescence enhancement, we discovered a robust adenosine 5'-triphosphate–powered dsRNA translocation activity of RIG-I. The CARDs dramatically suppress translocation in the absence of 5'-triphosphate, and the activation by 5'-triphosphate triggers RIG-I to translocate preferentially on dsRNA in cis. This functional integration of two RNA molecular patterns may provide a means to specifically sense and counteract replicating viruses.

Retinoic acid inducible–gene I (RIG-I) is a cytosolic pattern-recognition receptor that senses pathogen-associated molecular patterns (PAMPs) on viral RNA and triggers an antiviral immune response by activating type-I

interferons (IFN- α and - β) (1). A 5'-triphosphate moiety on viral RNA is a major PAMP detected by RIG-I as a viral signature (2, 3). 5'-triphosphates arise during viral replication and are absent in most cytosolic RNA because of cleavage or capping